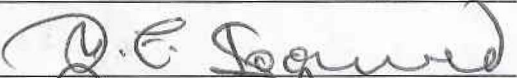


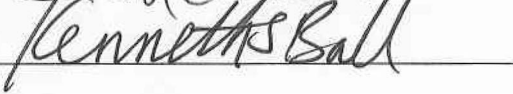
TWO-DIMENSIONAL MATERIALS: DOPING-INDUCED VARIATION,
HETEROJUNCTION FETS AND HYBRID MULTILAYERS

by

Kwesi P Eshun
A Thesis
Submitted to the
Graduate Faculty
of
George Mason University
in Partial Fulfillment of
The Requirements for the Degree
of
Master of Science
Electrical Engineering

Committee:

Dr. Qiliang Li, Thesis Director

Dr. Dimitris Ioannou, Committee Member

Dr. Jim Jones, Committee Member

Dr. Andre Manitius, Department Chair

Dr. Kenneth S. Ball, Dean, Volgenau School
of Engineering

Date: August 28, 2014

Summer Semester 2014
George Mason University
Fairfax, VA

Two-Dimensional Materials: Doping-Induced Variation, Heterojunction FETs and
Hybrid Multilayers

A thesis submitted in partial fulfillment of the requirements for the degree of Master of
Science at George Mason University

By

Kwesi P Eshun
Bachelor of Science
Kwame Nkrumah University of Science and Technology, 2011

Director: Qiliang Li, Associate Professor
Electrical and Computer Engineering Department

Summer Semester 2014
George Mason University
Fairfax, VA

DEDICATION

To my family for their unbounded love and to my advisors and department chair for their support.

TABLE OF CONTENTS

	Page
LIST OF FIGURES	iv
ABSTRACT	v
I. INTRODUCTION	1
II. COMPUTATIONAL METHOD	5
III. DOPING EFFECT ON TWO-DIMENSIONAL TMDS	6
IV. TWO-DIMENSIONAL HETEROJUNCTION	9
V. MoS ₂ /WSe ₂ HETEROJUNCTION FIELD EFFECT TRANSISTOR.....	12
VI. HYBRID MULTILAYER TMDS	17
VII. CONCLUSION	21
VIII. REFERENCES.....	23

LIST OF FIGURES

Figure	Page
FIG. 1: 10×10 MoS ₂ monolayer with one P atom	7
FIG. 2: Variation of band gap and sheet resistance against a) monolayer size b) number of dopants for 5×10 MoS ₂ monolayer	8
FIG. 3: Single layer of WSe ₂ and single MoS ₂ forming a bilayer of MoS ₂ /WSe ₂	9
FIG. 4: Stacking of MoS ₂ /WSe ₂ bilayer	10
FIG. 5: The calculated current-voltage characteristics at 300K of the constructed p-n junction	10
FIG. 6: MoS ₂ /WSe ₂ Heterojunction FET with gate.....	13
FIG. 7: Id-Vg curves for: a) 8nm channel length c) 10nm channel length Id-Vd curves for: b) 8nm channel length d) 10nm channel length.....	14
FIG. 8: Transmission spectra for 8nm channel length and 10nm channel length.....	15
FIG. 9: a) Bilayer of monolayer WSe ₂ and monolayer MoS ₂ b) 3 layers – 2 monolayers of WSe ₂ and monolayer MoS ₂ c) 4 layers – 3 monolayers of WSe ₂ and monolayer MoS ₂ d) 5 layers – 4 monolayers WSe ₂ and monolayer MoS ₂	18
FIG. 10: Bandstructure of bilayer and 3 layers.....	19
FIG. 11: Bandstructure of 4 layers and 5 layers	19
FIG. 12: Graph of band gap and effective mass versus multilayer.....	20

ABSTRACT

TWO-DIMENSIONAL MATERIALS: DOPING-INDUCED VARIATION, HETEROJUNCTION FETS AND HYBRID MULTILAYERS

Kwesi P Eshun, M.S.

George Mason University, 2014

Thesis Director: Dr. Qiliang Li

As the size of Complementary Metal Oxide Semiconductor (CMOS) field effect transistor (FET) approaches its fundamental physical limit, two-dimensional (2D) layered structures, such as transitional metal dichalcogenides (TMDs), have been proposed as the alternative channel materials to extend the Moore's law. In this thesis, we proposed and studied a new set of device structures based on 2D MoS₂/WSe₂ heterojunction in order to construct the smallest field effect transistor, whereas the switching is achieved via gated heterojunction. Following a step-by-step approach, we have studied the doping effect of different TMDs, formation of heterojunction between different TMDs and gated field effect transistor based on these 2D heterojunctions.

During the study of Doping effect on 2D TMDs, we found that random dopant position led to large variation in electronic properties of 2D materials. Therefore, we focus on the study of 2D heterojunction FET instead of the pn-junction. We have studied the formation and transport properties of 2D heterojunctions, with a focus on

MoS₂/WSe₂ heterojunction as it exhibits the best junction characteristics. We then used the MoS₂/WSe₂ heterojunctions as the channel materials to construct the smallest FET. Such 2D junction-based FETs exhibited very interesting and attractive device characteristics. This study has successfully demonstrated a new set of device structures and materials in order to achieve 2D FET for the extension of CMOS scaling. The results of this thesis may open a suit of new applications in future electronics.

I. INTRODUCTION

In recent years two dimensional (2D) materials have attracted a growing interest for their potential applications in future nanoelectronics [1]. The 2D materials have unique electrical, optical and mechanical properties which arise from the 2D crystal structure and ultrathin atomic-layer body [2]. After the discovery of graphene, atomically thin layered materials have been investigated as alternate channel materials in Metal-Oxide-Semiconductor Field Effect Transistor (MOSFET) due to their excellent electrostatic integrity, planar structure, and mechanical flexibility [3]. Graphene is the most cited 2D layered materials in these recent years. However, pristine graphene lacks a bandgap (E_g). As a result, transistors made from graphene cannot be effectively switched off and have low current on/off ratio.

The 2D Transition Metal Dichalcogenides (TMDs), such as MoS_2 , WS_2 and WSe_2 , offer properties different with graphene. TMDs belong to a class of materials with the formula MX_2 , where M is a transition metal element from group IV, group V or group VI and X is a chalcogen (S, Se or Te). They are composed of stacks of multiple X-M-X layers. One XM-X layer (monolayer MX_2) consists of an M atom layer sandwiched between two X atom layers. The M-X bonding is strongly covalent, but the X-M-X layers are coupled only by weak van der Waals forces [4]. Most 2D TMDs have sizable bandgaps around 1

eV to 2 eV, which is good for application in computational electronics and optoelectronics [5].

The overall symmetry of TMDs is hexagonal or rhombohedral, and the metal atoms have octahedral or trigonal prismatic coordination [1]. The electronic properties of TMDs range from metallic to semiconducting [1]. The layer-dependent properties of TMDs have recently attracted a great deal of attention. For example, in several semiconducting TMDs there is a transition from an indirect bandgap in the bulk to a direct gap in the monolayer. For example, bulk MoS₂ (with multiple layers) has an indirect bandgap of 1.20 eV, while MoS₂ monolayer has a direct bandgap of 1.80 eV [6]. For example, bulk WSe₂ has an indirect bandgap of 1.20 eV, while WSe₂ monolayer has a direct bandgap of 1.60 eV. Furthermore, the direct bandgap in monolayer of TMDs will lead to enhanced photoluminescence and photoelectric effect, which open many opportunities in optoelectronic applications [6].

In conventional microelectronic technology, doping the semiconductor body to increase either electron or hole concentration is considered to be essential to construct various devices, such as pn junction diode, solar cell, bipolar junction transistor (BJT) and MOSFET. [7] However, as the device dimensions are being shrunk to nanoscale, ultra-thin, it is difficult to control the level and position of dopant for the desired device properties.

In addition, engineering the properties of electronic devices with heterojunction is one of the important methods in semiconductor technology. The wide variety of truly 2D layered atomic crystals, such as graphene, MoS₂, WS₂, WSe₂ and MoSe₂, can be designed and integrated for various heterostructure for different application [8]. However, in the current stage, the research on heterojunction based on 2D materials has not yet been much explored.

In this thesis, we first studied the doping effect on the 2D MoS₂ nanoribbons. We found that the electrical properties of MoS₂ nanoribbons exhibited large variation due to the doping positions and doping level (1 to 3 dopants). Since it is physically difficult to control the position of dopant atom and the number of a few dopant atoms, we concluded that it is not to avoid significant device-to-device variation which is not allowed for very large-scale integrated circuit. Then, we studied the formation of heterojunction between two different TMDs. Our focus is on MoS₂/WSe₂ heterojunction as MoS₂ and WSe₂ are the most frequently cited TMDs. With the result of heterojunction, we integrated MoS₂/WSe₂ heterojunction with a gate on the junction to form field-effect transistors. This TMD-based transistor can operate in both the electron and hole-accumulation modes, depending on the polarity of the gate voltage. This ambipolar operation is rarely observed in high-mobility FETs [9]. MoS₂ monolayer based transistors have been recently demonstrated to operate at room temperature, with a mobility of at least 200 cm²/Vs and on/off current ratios of 10⁸ with low standby power dissipation [10] and

exhibits an n-type behavior [10]. Similarly, the mobility of the field-induced holes in WSe₂ monolayer based transistors has also been reported to be ~500 cm²/V s at room temperature and exhibits a p-type behavior [11]. In comparison, our MoS₂/WSe₂ heterojunction FET exhibit electron mobility 128cm²/V-s and hole mobility 117cm²/V-s. Overall, our study reports the first 8-nm heterojunction FET based on 2D layered materials with very promising applications for future devices. At last, we have also studied the construction of hybrid multilayer TMDs with direct band gap. These materials are interesting for optoelectronic application, such as solar cell.

II. COMPUTATIONAL METHOD

The calculations were performed by using the Perdew-Burke-Ernzerhof's[13] version of generalized gradient approximation in Atomistix Toolkit (ATK) [12] to describe the exchange correlation density functional. In our calculations double- ζ polarized[14] numerical atomic orbitals basis sets are used for all atoms. An equivalent plane wave cutoff of 150 Ry is used for the real space mesh and the Brillouin zone is sampled over a $9 \times 9 \times 1$ Monkhorst-Pack k grid. Periodic boundary conditions are applied and a vacuum layer of $\geq 17\text{\AA}$ is placed above the monolayer to minimize the interaction between the adjacent periodic images. A temperature of 300 K is used when populating the electronic states with a Fermi distribution. Due to the strains introduced in the formation of the heterostructure, during the simulation the geometry is relaxed first by using Quasi-Newton[15] optimizer method where all the atoms are allowed to relax until any force is smaller than 0.05eV/\AA .

The relaxation of the bilayer of MoS₂ and WSe₂, which both have the same crystal structure and very dissimilar lattice constants (Table 1)[12], minimizes the strain defects in the structure and produces an almost equivalent lattice constants in the stacked monolayers from which the heterostructure FET can be formed.

III. DOPING EFFECT ON TWO-DIMENSIONAL TMDS

The richness in the electronic properties of two dimensional TMDS makes them an ideal platform for a multitude of applications [16]. We study the doping effect on 2D MoS₂ nanoribbon and particularly by substitutional doping rather than the possible creation of Mo and/or S vacancies since these vacancies will always produce deep trap states in the monolayer band gap [17]. We identify suitable dopants for making the nanoribbon either n-type or p-type when an S is substituted by phosphorus, P (p-type) or the metal, Mo is substituted by rhenium, Re (n-type) where rhenium is chosen a possible substitutional dopant at the Mo site due to its low activation energy [7] and a higher mixing of d-orbitals to provide extra electrons to enhance conductance. We realize p-type doping by substituting a S atom in different sites on the surface with a P atom. The dependence of bandgap and sheet resistance on the doping sites are investigated. Importantly, the substitution of S with P rigidly shifts the defect states closer to the valence band maximum (VBM) of the pristine MoS₂ monolayer. We observed little bandgap oscillation on the overall doping sites. However, the variation of the band gap on doping sites near the center of the MoS₂ nanoribbon is apparent. Conversely, the sheet resistance showed a more pronounced variation from the edge/base towards the center of the MoS₂ nanoribbon when doped with a single P atom.

Similar trends in the variation of the band gap and sheet resistance appears with more

dopants. However, decreasing the width of the MoS₂ nanoribbon shows a larger variation of the band gap and the sheet resistance on doping sites, in spite of the number of dopants.

Next we consider substitutional doping at the Mo site with a different transition metal. Re (*5d*) is our favored choice because it possesses growing number of *d* shell electrons with larger *d* occupancy than Mo, leading to higher mixing of *d* shell electrons. This highly mixed electrons in *d* shell remains unpaired, which attributes to higher conductance of doped nanoribbon by substitution of Re on Mo. Re donor level is located at 0.18eV below the conduction band minimum (CBM) which is consistent to the similar reported calculation[18][19] suggesting that Re could be used as n-type dopant in the MoS₂ nanoribbon.

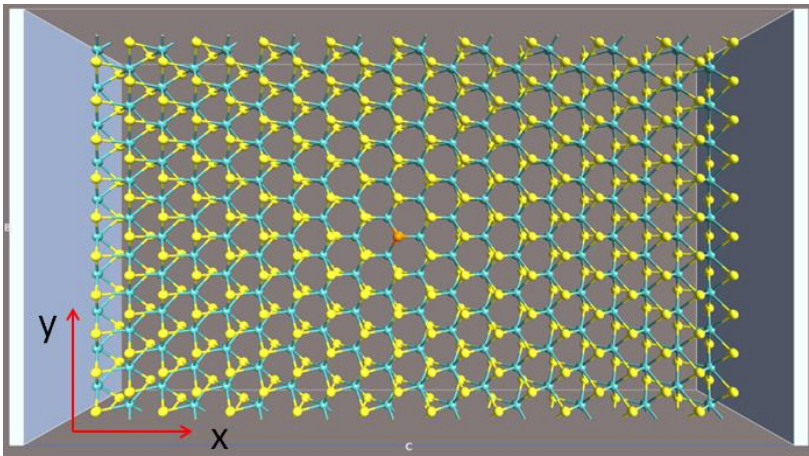
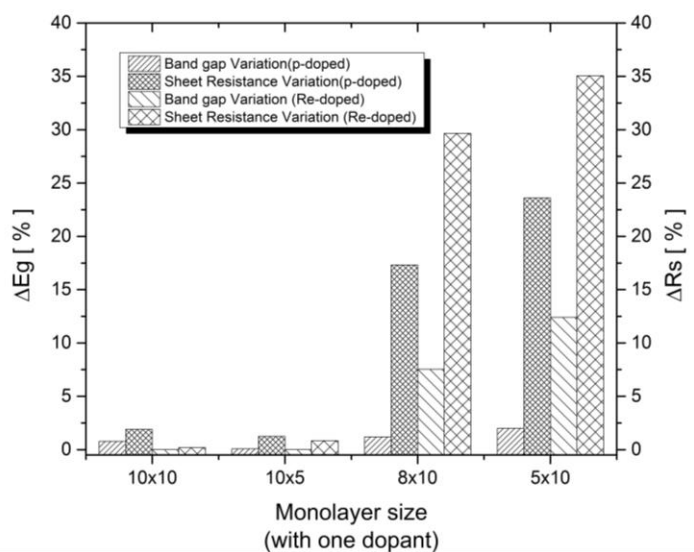
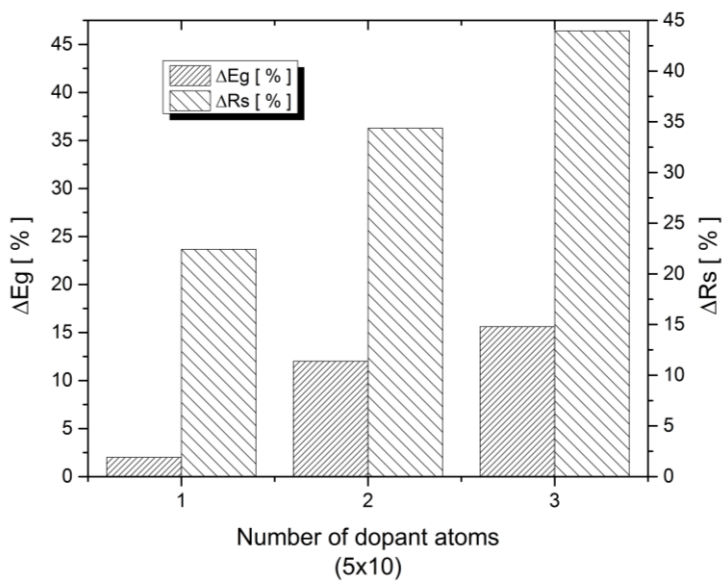


FIG. 1 10×10 MoS₂ monolayer with one P atom



a.



b.

FIG. 2 a) Variation of band gap and sheet resistance against monolayer size
 b) Variation of band gap and sheet resistance against number of dopant atoms for 5x10 MoS₂ monolayer

IV. TWO-DIMENSIONAL HETEROJUNCTION

Engineering the electronic properties of semiconductors by using heterojunctions has been a central concept in semiconductor science and technology for decades [20]. More recently, the study of electronic and optoelectronic devices based on a single MoS_2 layer and WSe_2 layer has been given much attention due to their intrinsic direct band gap nature and their fabrication of a high mobility field effect transistor based on a single layer MoS_2 and single layer WSe_2 . Here, we report results on the stacking of the different TMD monolayers forming a field effect transistor with electronic properties and device characteristics different from the homogeneous TMD monolayers

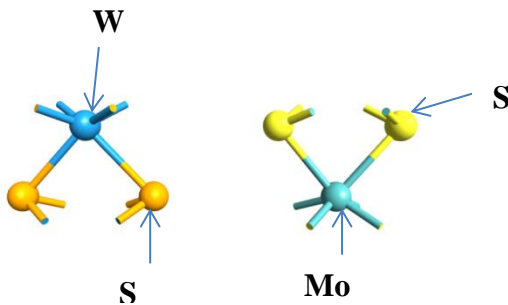


FIG. 3 Single layer of WSe_2 and single MoS_2 forming a bilayer of $\text{MoS}_2/\text{WSe}_2$

Stacking of the $\text{MoS}_2/\text{WSe}_2$ is achieved by chemical bonding of the single layer TMD (FIG. 5) creating a junction between the different single layer TMDs. We then analyze the I-V characteristic of the junction formed.

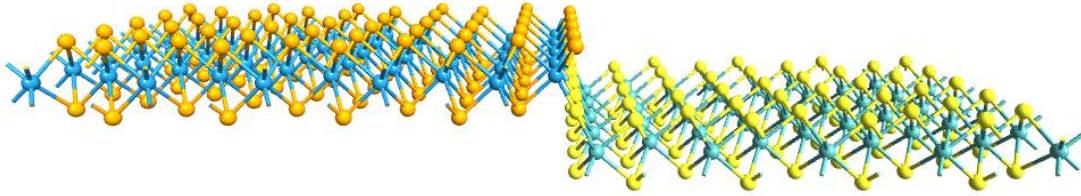


FIG. 4 Stacking of $\text{MoS}_2/\text{WSe}_2$ bilayer

DIODE BEHAVIOR

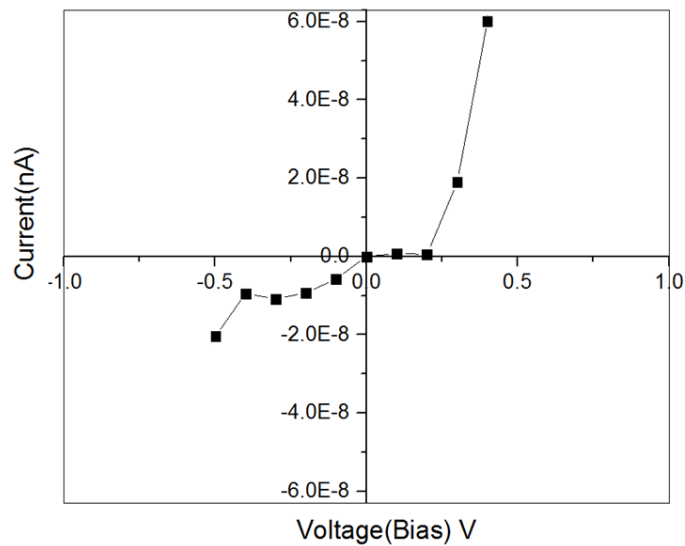


FIG. 5 The calculated current-voltage characteristics at 300K of the constructed p-n junction

The diode exhibits excellent rectification behavior and a low reverse bias current, suggesting high quality interfaces between the stacked layers. We then use this heterojunction to construct a field effect transistor and investigate the transport properties and device characteristics of a gated field effect transistor. The field effect transistor constructed exhibits an n-type behavior with different channel lengths of 8nm-10nm.

V. MoS₂/WSe₂ HETEROJUNCTION FIELD EFFECT TRANSISTOR

In this system, all interfaces are based on Van-der-Waal's bonding, presenting a unique device architecture where crystalline, layered materials are stacked on demand, without the lattice parameter constraints[21]. We consider the full band effects on the limits of ballistic transport in n-channel MoS₂/WSe₂ heterojunction FET via atomistic quantum transport simulations. The simulated device structure is illustrated in Fig. 6. We consider 8nm and 10nm channel lengths with single, double and triple junction overlaps. For Non-Equilibrium Green Function (NEGF) in ATK, a multi-grid poisson solver is employed using Dirichlet boundary conditions on the left and right faces (i.e., the electrodes) and Neumann boundary conditions on the other faces (i.e., transport direction) of the device. The electrode temperatures are considered 300 K. The carrier densities evaluated from the NEGF formalism are put into the Poisson solver to evaluate a more accurate guess of the self-consistent potential, U_{SCF} and the same is used to evaluate a more accurate value of number density of carriers[22]. The I-V characteristics are calculated using the NEGF formalism[23][24] . In the NEGF method, we proceed to solve the-Poisson Schrödinger equation of the system (Fig. 6). The ballistic drain current which is calculated by integrating transmission coefficients over energy with a Fermi function weight is given as[23][24]:

$$I = \left(\frac{4e}{h}\right) \int_{-\infty}^{+\infty} \delta(E, V) [f_s(Ek, x - \mu_s) - f_d(Ek, x - \mu_d)] dE \quad (1)$$

In Eq. (1) e is the electronic charge, f_s and f_d are the Fermi functions in the source and drain contacts, μ_s and μ_d are the source and drain chemical potentials, respectively and h is the Planck's constant . The factor 4 originates from the spin degeneracy and valley degeneracy[22] and the equation holds good for short channel lengths below 15nm[24]

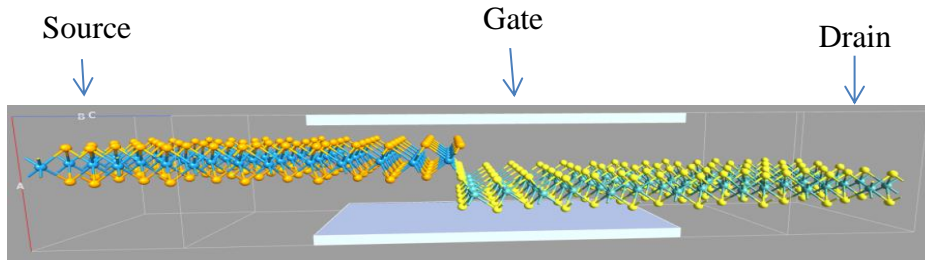


FIG. 6 MoS₂/WSe₂ Heterojunction FET with gate.

Device Characteristics

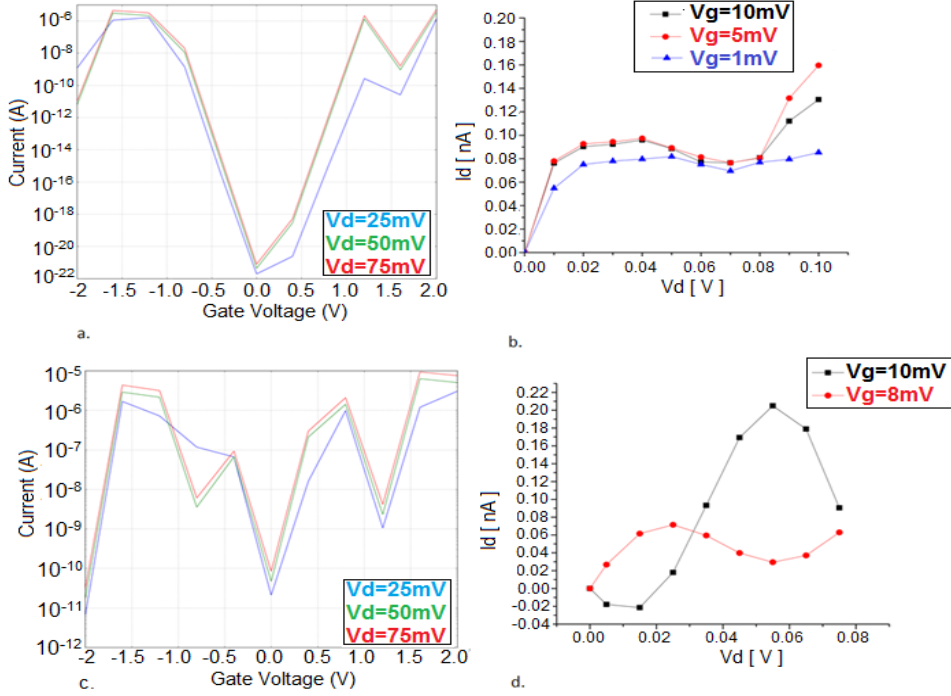


FIG. 7 Id-Vg curves for: a) 8nm channel length c) 10nm channel length
Id-Vd curves for: b) 8nm channel length d) 10nm channel length

In FIG. 7 b) and d) we see the Id – Vd characteristics of the MoS₂/WSe₂ Heterojunction FET characteristics under gate bias. The curve displays slight negative differential resistance characteristics of the device under a drain bias sweep from 0V to 0.1V in b) with varying gate bias of 1mV, 5mV and 10mV. Similarly, d) also displays such a characteristic under a drain bias sweep from 0V to 0.08V with varying gate bias of 8mV

and 10mV. In a) and c) we see the I_d - V_g characteristics of the $\text{MoS}_2/\text{WSe}_2$ Heterojunction FET characteristics under varying drain bias of 25mV, 50mV and 75mV. In order to explain the behavior of the I_d - V_d curves for the 8nm and 10nm channel lengths we first consider the transmission spectra of the devices. It is observed for the 8nm channel length that for a fixed gate bias of 5mV, as a small drain bias is applied more number of transmission modes appear near the Fermi level of the channel, which indicates a greater transmission transparency of the channel. As the drain voltage is increased further, the some of the transmission modes near the Fermi level seem to be less suppressed. This leads to a slight drop in the transmission transparency of the channel, thus indicating the slight negative resistance behavior[21][22]. A similar phenomenon occurs in the 10nm channel length for a fixed gate bias of 10mV.

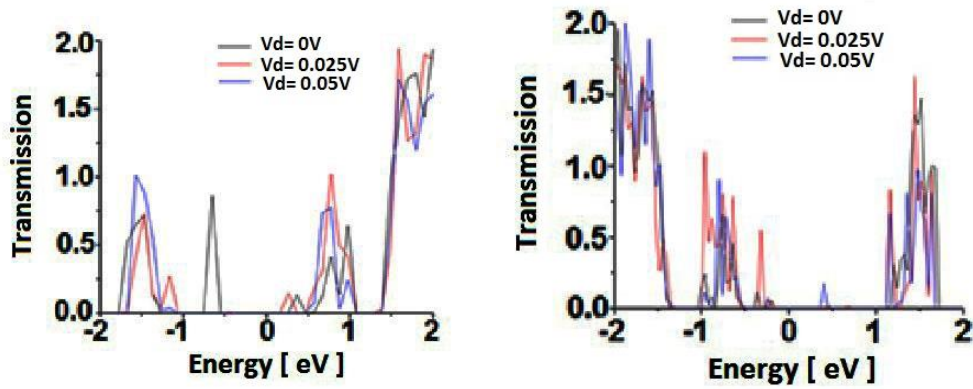


FIG. 8 Transmission spectra for 8nm channel length (left) and 10nm channel length (right)

We now look to understand the behavior of the decreasing current in the devices for a drain bias range of $0V \leq Vd \leq 0.075V$. This negative differential resistance (NDR) can be related to the formation convoluted semiclassical conduction paths between source and drain[25]. We however note that the region of NDR in Vd will depend on the location of the Fermi level in the bandstructure, which is used as the energy reference and also the carrier concentrations. That is, a higher or lower carrier concentration will reduce or increase, respectively, the magnitude of NDR onset Vd somewhat[23][25].

The convoluted semiclassical trajectory of the electron requires the electron to first accelerate toward the drain, then decelerate, turn around, accelerate back toward the source, decelerate again, and turn back around, before finally accelerating back to and out of the drain. Quantum mechanically, the overall right-propagating state nominally incorporates a superposition of two right-going waves of different wavelengths and one left-going wave of yet another wavelength over a significant portion of the channel, making for a less adiabatic transition between source and drain[25]. Additionally, an overall velocity reduction in the channel associated with this convoluted trajectory can be expected to affect somewhat the self-consistent electrostatics considered in the simulations.

However the I_d - V_d curve for the 10nm channel shows a higher peak-to-valley ratio (PVR) than in the 8nm channel length. That is the PVR in the 8nm channel length is ≤ 1.2 which means the negative differential resistance is significantly suppressed.

VI. HYBRID MULTILAYER TMDS

We show that TMD multilayer offer a direct band gap and tunable electronic structures by first principles of electronic structure theory. The tunability is achieved by the thickness ratio of the multilayers across the hetero-interface[26]. One of the primary advantages of layered materials is, in principle, the absence of dangling bonds, which rules out performance degradation due to interface states[27]. Uniquely, heterostructures using two-dimensional materials would not suffer from constraints of lattice mismatch. A layered material can be seamlessly transferred onto another, and bond by Van-der-Waal's (vdW) forces, leaving the interface pristine. In order to have a tunable band gap for a more powerful TMD optoelectronics we periodically stack monolayers of WSe₂ on a monolayer of MoS₂ as can be seen in FIG. 9 and the band gap remains direct but when we periodically repeat hetero-bilayers to form a superlattice, an indirect gap emerge. It is observed that the associated in-layer lattice constant a varies from 3.1604Å to 3.282Å, for the monolayers of MoS₂ and WSe₂ respectively, However when the monolayers are stacked, the in-layer lattice constant a , of the MoS₂/WSe₂ formed is 3.282Å close to that of the monolayer of WSe₂ suggesting that the band gap of multilayer will remain direct. Similarly, the lattice parameter c of MoS₂/WSe₂ stays close to that of monolayer WSe₂. The tuning of the band gaps can be explained by the stacking and the valence band (VB) separations. As WSe₂ in the multilayer becomes thicker, there is a larger VB separation at

the K point, hence the smaller the K→K direct band gap. It can then be inferred that the conduction bands are solely contributed by the conduction band of MoS₂ and also the valence band(s) originates from the valence band(s) of WSe₂. However, the multilayer bands formed are simply a superposition of the monolayer states.

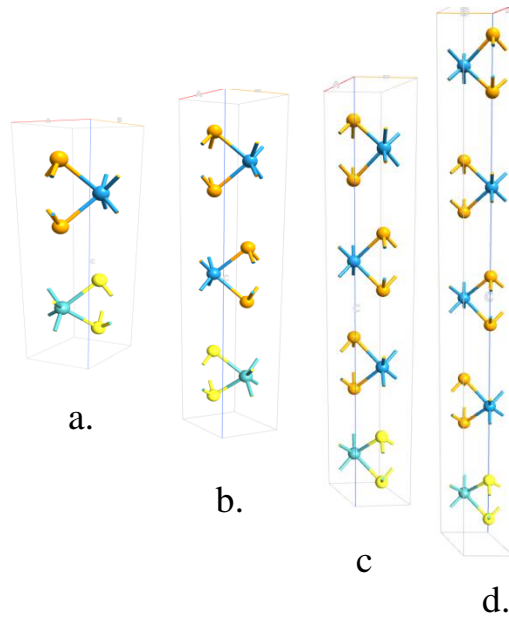


FIG. 9 a) Bilayer of monolayer WSe₂ and monolayer MoS₂ b) 3 layers – 2 monolayers of WSe₂ and monolayer MoS₂ c) 4 layers – 3 monolayers of WSe₂ and monolayer MoS₂ d) 5 layers – 4 monolayers WSe₂ and monolayer MoS₂.

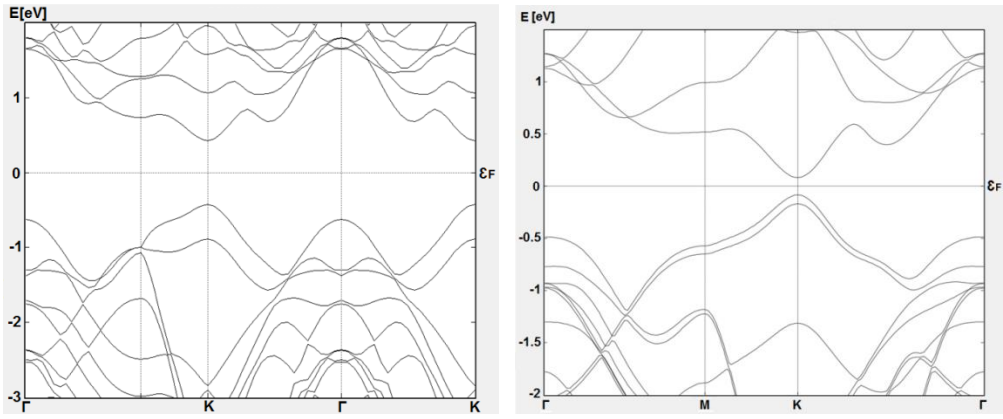


FIG. 10 Bandstructure of bilayer (left) and 3 layers (right)

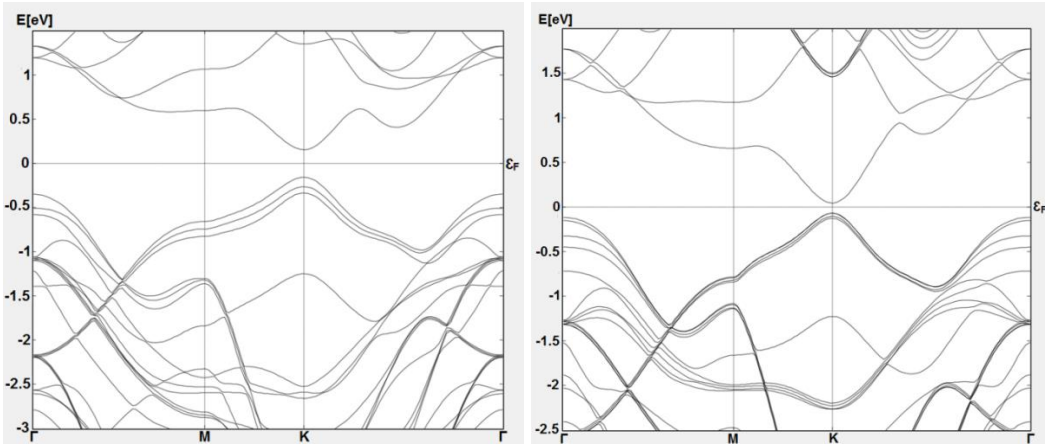


FIG. 11 Bandstructure of 4 layers (left) and 5 layers (right)

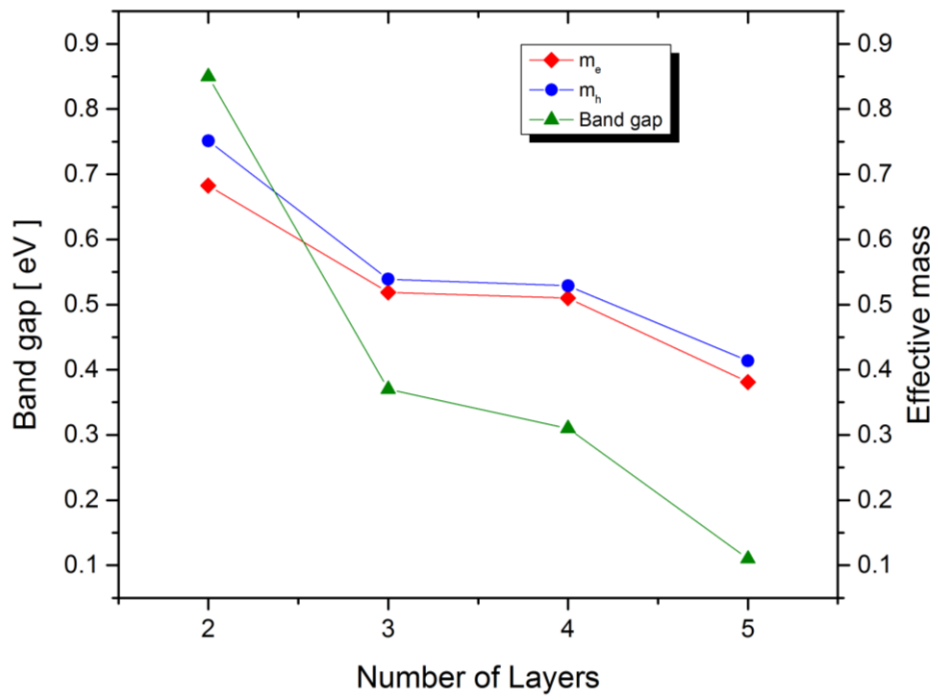


FIG. 12 Graph of band gap and effective mass versus multilayer

VII. CONCLUSION

We used atomistic full-band quantum transport simulations for the output characteristics of the p-n junction and the heterojunction field effect transistor. We have observed that the p-n junction diode of the MoS₂-WSe₂ heterojunction exhibits clear rectification behavior and the low reverse bias current suggest high interface quality between MoS₂ and WSe₂ with minimal lattice constraints. More importantly, the van-der-Waal (vdW) bonding of the interfaces provide pathways for making complex devices based on crystalline layers without lattice parameters constraints[23]. Additionally, the diode gives an example of configuring layered material components into functional device through the multi-step transfer process.

The MoS₂/WSe₂ heterojunction field effect transistor demonstrates clear n-type switching behavior with on/off current ratio of $> 10^6$ and with the 8nm channel length exhibiting good subthreshold slopes as well as small drain-induced-barrier lowering (DIBL). This characteristic of the device may be attributed to the electrostatic control afforded by the two-dimensional nature of the MoS₂/WSe₂ heterostructure.

In this simulation, calculations are performed in the ballistic limit of transport and the presence of scattering would substantially affect the ON-state transconductance as well as the aforementioned NDR behavior. With the presence of scattering, intra-band source-to-drain transport even when not otherwise possible (or at least improbable allowing for

band-to-band tunneling) may be allowed by dissipating energy in the channel, and perhaps by adding additional inter-band transport paths[25]. Therefore, scattering would increase the current beyond the nominal NDR onset voltages in addition to reducing ON-state current under lower V_d , thereby, reduce or eliminate the NDR [25][28]. In this way, the differences in transconductance among materials at higher V_d also likely will be reduced substantially by scattering. However, limited NDR could serve as a signature of quasi-ballistic transport in nanoscale TMD FETs [4][22].

For the hybrid multilayer TMD, the introduction of strain affects the band gaps of TMD and might change the dominant band gap from direct to indirect but our hybrid multilayer resists such change and we conclude that they are quite robust against strain as far as the direct band gap is concerned [29]. We also note that in the case of the MoS₂/WSe₂ multilayer, weak interlayer coupling competes with the energy difference of the monolayer states and as a result the VBM is at the K point. More importantly we find that the lowest energy electron and highest energy hole states in the optically active K point are localized on different monolayers. Photoluminescence in this hybrid multilayer TMD can be achieved due to the availability of photoexcited holes at the K point. Additionally, the spatially separated valance and conduction bands which is a desirable property would help to reduce recombination of electron-hole pairs and lead to higher quantum efficiency of photoelectron generation[29]. Finally, we introduce the issue of band gap engineering in the hybrid multilayer which holds a promising application in optoelectronic and photovoltaic systems and a bright future for optospintronics.

VIII. REFERENCES

- [1] Q. H. Wang, K. Kalantar-Zadeh, A. Kis, J. N. Coleman, and M. S. Strano, “Electronics and optoelectronics of two-dimensional transition metal dichalcogenides,” *Nat. Nanotechnol.*, vol. 7, no. 11, pp. 699–712, 2012.
- [2] A. M. Iskandarov and S. V. Dmitriev, “Thermoactivated fracture of graphene subjected to tensile strain,” *Tech. Phys. Lett.*, vol. 39, no. 2, pp. 185–188, 2013.
- [3] R. K. Ghosh and S. Mahapatra, “Direct Band-to-Band Tunneling in Reverse Biased Nanoribbon pn Junctions,” *Electron Devices IEEE Trans. On*, vol. 60, no. 1, pp. 274–279, 2013.
- [4] J. Chang, L. F. Register, and S. K. Banerjee, “Comparison of ballistic transport characteristics of monolayer transition metal dichalcogenides (TMDs) MX_2 (M= Mo, W; X= S, Se, Te) n-MOSFETs,” in *Simulation of Semiconductor Processes and Devices (SISPAD), 2013 International Conference on*, 2013, pp. 408–411.
- [5] J. A. Wilson and A. D. Yoffe, “The transition metal dichalcogenides discussion and interpretation of the observed optical, electrical and structural properties,” *Adv. Phys.*, vol. 18, no. 73, pp. 193–335, 1969.
- [6] A. Kuc, N. Zibouche, and T. Heine, “Influence of quantum confinement on the electronic structure of the transition metal sulfide $T S_2$,” *Phys. Rev. B*, vol. 83, no. 24, p. 245213, 2011.
- [7] K. Dolui, I. Rungger, C. D. Pemmaraju, and S. Sanvito, “Possible doping strategies for MoS_2 monolayers: An ab initio study,” *Phys. Rev. B*, vol. 88, no. 7, p. 075420, 2013.
- [8] A. Ferreira and N. M. R. Peres, “Complete light absorption in graphene-metamaterial corrugated structures,” *Phys. Rev. B*, vol. 86, no. 20, p. 205401, 2012.
- [9] V. Podzorov, M. E. Gershenson, C. Kloc, R. Zeis, and E. Bucher, “High-mobility field-effect transistors based on transition metal dichalcogenides,” *Appl. Phys. Lett.*, vol. 84, no. 17, pp. 3301–3303, 2004.

- [10] B. Radisavljevic, A. Radenovic, J. Brivio, V. Giacometti, and A. Kis, “Single-layer MoS₂ transistors,” *Nat. Nanotechnol.*, vol. 6, no. 3, pp. 147–150, 2011.
- [11] H. Fang, S. Chuang, T. C. Chang, K. Takei, T. Takahashi, and A. Javey, “High-performance single layered WSe₂ p-FETs with chemically doped contacts,” *Nano Lett.*, vol. 12, no. 7, pp. 3788–3792, 2012.
- [12] Q. Simulator, *Atomistix ToolKit (ATK)*. 2012.
- [13] J. P. Perdew, K. Burke, and M. Ernzerhof, “Generalized gradient approximation made simple,” *Phys. Rev. Lett.*, vol. 77, no. 18, p. 3865, 1996.
- [14] J. Junquera, Ó. Paz, D. Sánchez-Portal, and E. Artacho, “Numerical atomic orbitals for linear-scaling calculations,” *Phys. Rev. B*, vol. 64, no. 23, p. 235111, 2001.
- [15] D. F. Shanno, “Conditioning of quasi-Newton methods for function minimization,” *Math. Comput.*, vol. 24, no. 111, pp. 647–656, 1970.
- [16] D. Jerome, A. J. Grant, and A. D. Yoffe, “Pressure enhanced superconductivity in NbSe₂,” *Solid State Commun.*, vol. 9, no. 24, pp. 2183–2185, 1971.
- [17] J. D. Fuhr, A. Saúl, and J. O. Sofo, “Scanning Tunneling Microscopy Chemical Signature of Point Defects on the MoS₂ (0001) Surface,” *Phys. Rev. Lett.*, vol. 92, no. 2, p. 026802, 2004.
- [18] J. Chang, “Ab-initio electronic structure and quantum transport calculations on quasi-two-dimensional materials for beyond Si-CMOS devices,” 2013.
- [19] M. R. Komarneni, Z. Yu, U. Burghaus, Y. Tsvetin, A. Zak, Y. Feldman, and R. Tenne, “Characterization of Ni-Coated WS₂ Nanotubes for Hydrodesulfurization Catalysis,” *Isr. J. Chem.*, vol. 52, no. 11–12, pp. 1053–1062, 2012.
- [20] P. Y. Yu and M. Cardona, *Fundamentals of Semiconductors, 1999*. Springer, Berlin.
- [21] T. Roy, M. Tosun, J. S. Kang, A. B. Sachid, S. Desai, M. Hettick, C. C. Hu, and A. Javey, “Field-Effect Transistors Built from All Two-Dimensional Material Components,” *ACS Nano*, 2014.
- [22] A. Sengupta and S. Mahapatra, “Negative differential resistance and effect of defects and deformations in MoS₂ armchair nanoribbon metal-oxide-semiconductor field effect transistor,” *J. Appl. Phys.*, vol. 114, no. 19, p. 194513, 2013.
- [23] K. Natori, “Ballistic metal-oxide-semiconductor field effect transistor,” *J. Appl. Phys.*, vol. 76, no. 8, pp. 4879–4890, 1994.

- [24] S. Datta, *Quantum transport: atom to transistor*. Cambridge University Press, 2005.
- [25] J. Chang, L. F. Register, and S. K. Banerjee, “Ballistic performance comparison of monolayer transition metal dichalcogenide MX₂ (M= Mo, W; X= S, Se, Te) metal-oxide-semiconductor field effect transistors,” *J. Appl. Phys.*, vol. 115, no. 8, p. 084506, 2014.
- [26] Y.-H. Zhao, F. Yang, J. Wang, H. Guo, and W. Ji, “Continuously tunable electronic structure of transition metal dichalcogenides superlattices,” *ArXiv Prepr. ArXiv13107285*, 2013.
- [27] R. Ghosh and S. Mahapatra, “Monolayer Transition Metal Dichalcogenide Channel Based Tunnel Transistor,” 2013.
- [28] L. Liu, S. Bala Kumar, Y. Ouyang, and J. Guo, “Performance limits of monolayer transition metal dichalcogenide transistors,” *Electron Devices IEEE Trans. On*, vol. 58, no. 9, pp. 3042–3047, 2011.
- [29] K. Kośmider and J. Fernández-Rossier, “Electronic properties of the MoS₂-WS₂ heterojunction,” *Phys. Rev. B*, vol. 87, no. 7, p. 075451, 2013.

<C:\Users\SEvans\AppData\Local\Temp\bio.docx>

BIOGRAPHY

Kwesi P. Eshun graduated from Kwame Nkrumah University of Science and Technology in Ghana-West Africa, in 2011 where he received his Bachelor of Science in Physics. He worked as a Research Assistant for two years at George Mason University under the supervision of his advisors, Dr. Qiliang Li and Prof. Dimitris Ioannou in the field of Microelectronics and Nanotechnology.